Global Monsoon, El Niño, and Their Interannual Linkage Simulated by MIROC5 and the CMIP3 CGCMs

HYUNG-JIN KIM AND KUMIKO TAKATA

Research Institute for Global Change, Japan Agency for Marine-Earth Science and Technology, Kanagawa, Japan

BIN WANG

International Pacific Research Center, and Department of Meteorology, School of Ocean and Earth Science and Technology, University of Hawaii at Manoa, Honolulu, Hawaii

MASAHIRO WATANABE AND MASAHIDE KIMOTO

Atmospheric and Ocean Research Institute, University of Tokyo, Chiba, Japan

TOKUTA YOKOHATA

Center for Global Environmental Research, National Institute for Environmental Studies, Ibaraki, Japan

TETSUZO YASUNARI

Research Institute for Global Change, Japan Agency for Marine-Earth Science and Technology, Kanagawa, and Hydrospheric Atmospheric Research Center, Nagoya University, Nagoya, Japan

(Manuscript received 13 October 2010, in final form 23 February 2011)

ABSTRACT

This study evaluates the capability of coupled global climate models (CGCMs) in simulating the prime examples of the forced response (global monsoon) and internal feedback process (El Niño). Emphases are also placed on the fidelity of the year-to-year variability of global monsoon precipitation that is coordinated by the interannual sea surface temperature (SST) fluctuation over the tropics. The latest version of the Model for Interdisciplinary Research on Climate 5 (MIROC5) with advanced physical schemes is compared with the two previous versions (MIROC3.2, high- and medium-resolution versions) and with the 20 CGCMs participating in the third phase of the Coupled Model Intercomparison Project (CMIP3). The climatological annual mean and cycles of precipitation and 850-hPa winds, the key components to demarcate the global monsoon domain, are reproduced better in MIROC5 than in MIROC3 versions. As a consequence, the former considerably outperforms the latter and is generally superior to the CMIP3 CGCMs in replicating the intensity and domain of global monsoon precipitation and circulations. These results highlight the importance of the improved physical parameterization in a model. Analyses of the monthly Niño-3 index suggest that the amplitude and periodicity of El Niño are simulated better in MIROC5 than in the MIROC3 versions. Yet the reality of nonlinear ENSO dynamics measured indirectly by the SST asymmetricity over the equatorial Pacific is unsatisfactory in the MIROC family as well as in the majority of the CMIP3 models. The maximum covariance analysis shows that a significant fraction of the interannual global monsoon rainfall variability is in concert with El Niño. The multimodel results reveal that such coupling is robust across the current CGCMs. More importantly, the fidelity of the global monsoon precipitation significantly relies on the realism of tropical SST. Comparison among the MIROC models suggests that improved El Niño is likely attributable to the more realistic Bjerknes feedback loop, which results from the intensified convective activity over the equatorial central Pacific Ocean.

1. Introduction

Verifying and tracing the performance of a coupled global climate model (CGCM) is indispensable for its continuous improvement. These efforts can also provide

Corresponding author address: Hyung-Jin Kim, Research Institute for Global Change, JAMSTEC, 3173-25 Showa-machi, Kanazawa-ku, Yokohama, Kanagawa 236-0001, Japan.
E-mail: hyungjin@jamstec.go.jp

DOI: 10.1175/2011JCLI4132.1

valuable information from which the scientific community gains confidence in utilizing a CGCM for various purposes. The evaluation more often focuses on the fundamental processes of the climate system. The processes involved in the evaluation may be reasonably categorized into two groups, depending upon the type of impetus: forced responses to external forcings and self-recurrent phenomena due to internal feedbacks.

Solar radiation change on daily-to-orbital time scales is a typical example of the external forcings. It induces distinctive meteorological phenomena that are in phase with the temporal variation of the solar forcing. Among the diverse periodicities of the forced responses, however, emphasis could be placed on the annual cycle of precipitation and circulations since it manifests the global-scale monsoon, one of the profound meteorological events on the planet (Trenberth et al. 2000; Wang and Ding 2008). Internal feedback processes are complementary to the forced responses as they represent the natural fluctuations within the atmosphere or the coupled climate system. The El Niño–Southern Oscillation (ENSO) is often described as the most salient illustration of the internally organized modes of variability. Therefore, the fidelity of global monsoon and ENSO reproduced in a CGCM primarily reflects its skill in replicating forced responses and internal feedback processes.

El Niño is also known to exert enormous impacts on regional monsoon systems by modulating the onset, intensity, and retreat of monsoon precipitation (Tanaka 1997; Wu and Wang 2000; Annamalai et al. 2007; Vecchi and Wittenberg 2010). Traditionally, the effect of ENSO on interannual monsoon variability has been studied from a regional point of view. However, a concept of global monsoon has been recently proposed, by which the regional monsoons around the globe can be viewed as an integrated system (Wang and Ding 2006, 2008). Wang et al. (2011b, manuscript submitted to *Nat. Geosci.*) further demonstrated that the global monsoon precipitation, the rainfall amount falling into the global monsoon domain, displays a coherent year-to-year variability that is coordinated by ENSO. Though the internationally organized CGCM experiments and the accessible archive of the model outcomes have led to numerous research studies to assess the characteristics, physical processes, and feedbacks of ENSO in CGCMs (Neelin et al. 1992; Mechoso et al. 1995; Latif et al. 2001; AchutaRao and Sperber 2006; Joseph and Nigam 2006; Jin et al. 2008; Guilyardi et al. 2009), the extent to which a CGCM simulates the interannual relationship between global monsoon precipitation and ENSO is not investigated yet.

The present study aims to address the overall aspects of global monsoon climatology, El Niño properties and, in particular, year-to-year El Niño–global monsoon fluctuation simulated by the latest version of the Model for Interdisciplinary Research on Climate, MIROC5, in comparison with its predecessors, MIROC3(hires) and MIROC3(medres), and the Coupled Model Intercomparison Project phase 3 (CMIP3) CGCMs. MIROC5 was developed jointly at the Center for Climate System Research at the University of Tokyo, National Institute for Environmental Studies, and the Japan Agency for Marine-Earth Science and Technology. To date, one realization for the Twentieth-Century Climate in Coupled Model (20C3M) simulations has been conducted by using T85 atmospheric and approximately 1° ocean models. The atmospheric resolution of MIROC5 is between the two versions of MIROC3 [MIROC3(medres) and MIROC3(hires) with T42 and T106 atmospheric components, respectively]. But its oceanic component has the same resolution with MIROC3(medres). In general, the MIROC5 grid system is close to that of MIROC3(medres). Most of the physical parameterizations in MIROC5 are upgraded or replaced with new schemes, whereas the atmospheric dynamical core remains nearly intact. Readers may refer to Watanabe et al. (2010) for a comprehensive description of MIROC5.

The MIROC versions have been widely used to study decadal-to-centennial changes in the coupled atmosphere–ocean system (van Oldenborgh et al. 2005; Lin 2007; Wang et al. 2009) and over the ocean surface (Polito et al. 2008), extreme climates (Shiogama et al. 2008; Sugiyama et al. 2010), and climate change and carbon cycle (Yokohata et al. 2007; Yoshikawa et al. 2008). Although various atmospheric and oceanic aspects of mean states, time-dependent variability, and climate sensitivity reproduced by the MIROCs have been previously explored, the realism in simulating global monsoon and its linkage with El Niño has not been addressed yet. In particular, a brief analysis on El Niño property carried out by Watanabe et al. (2010) showed much more realistic El Niño amplitude in MIROC5 than in MIROC3. Considering the instrumental role of El Niño on regional monsoons as stated above, this suggests that the impacts of El Niño on global monsoon precipitation which is, in essence, the integral of all of the subregional and regional monsoons, may differ between the old and new models and thus deserve further investigation.

We first describe the data and models used in this study in section 2. Section 3 validates the fidelity of the simulated global monsoon with the aid of the diagnostic metrics designed and proposed by Wang et al. (2011a). Section 4 examines model ability in representing the essential characteristics of El Niño, such as amplitude, asymmetricity, and periodicity. In section 5, the year-to-year coupling between global monsoon precipitation and El Niño is extracted from the model outputs by using

TABLE 1. A list of the 23 CMIP3 CGCMs used in this study.

Model	Resolution	
	Atmosphere[a] (°)	Ocean[b]
1. CGCM3.1-T47 (Canada)	3.75 × ~3.75	192 × 96
2. CGCM3.1-T63 (Canada)	2.8125 × ~2.8125	256 × 192
3. CNRM-CM3 (France)	2.8125 × ~2.8125	180 × 170
4. CSIRO Mk3.0 (Australia)	1.875 × ~1.875	192 × 189
5. CSIRO Mk3.5 (Australia)	1.875 × ~1.875	192 × 189
6. GFDL CM2.0 (United States)	2.5 × 2.0	360 × 200
7. GFDL CM2.1 (United States)	2.5 × ~2	360 × 200
8. GISS-AOM (United States)	4 × 3	90 × 60
9. GISS-EH (United States)	5 × 4	72 × 46
10. GISS-ER (United States)	5 × 4	72 × 46
11. IAP FGOALS-g1.0 (China)	2.8125 × ~3	360 × 170
12. INM-CM3.0 (Russia)	5 × 4	144 × 84
13. IPSL CM4 (France)	3.75 × ~2.5	180 × 170
14. MIUBECHOG (Germany/Korea)	3.75 × ~3.75	128 × 117
15. MPI ECHAM5 (Germany)	1.875 × ~1.875	360 × 180
16. MRI CGCM2.3.2a (Japan)	2.8125 × 2.8125	144 × 111
17. NCAR CCSM3 (United States)	1.40625 × ~1.40625	320 × 395
18. NCAR PCM (United States)	2.8125 × ~2.8125	360 × 180
19. UKMO HadCM3 (United Kingdom)	3.75 × 2.5	288 × 144
20. UKMO HadGEM1 (United Kingdom)	1.875 × ~1.25	360 × 216
21. MIROC3.2(hires)[c] (Japan)	1.125 × ~1.125	320 × 320
22. MIROC3.2(medres)[d] (Japan)	2.8125 × ~2.8125	256 × 192
23. MIROC5 (Japan)	1.40625 × ~1.40625	360 × 180

[a] Longitude × latitude.
[b] Number of grids in longitude and latitude.
[c] MIROC3(hires) in this study.
[d] MIROC3(medres) in this study.

the maximum covariance analysis (MCA) (Bretherton et al. 1992) and compared with the observed—with particular emphasis on the MIROC5 integration. In addition, the mechanism that is possibly responsible for the differing El Niño simulations among the MIROC versions is discussed. Concluding remarks are presented in the last section.

2. Data and models

A 30-yr climatology from the Global Precipitation Climatology Project (GPCP) (Adler et al. 2003) over 1979–2008 and National Centers for Environmental Prediction–Department of Energy Reanalysis 2 (R2) (Kanamitsu et al. 2002) over 1980–2009 was constructed to verify climatological monsoon precipitation and circulations. For the validation of El Niño and its interannual linkage with global monsoon precipitation, the GPCP and the NOAA Extended Reconstruction Sea Surface Temperature (ERSST), version 3, (Smith et al. 2008) datasets for the period of 1979–2008 were utilized.

To facilitate model-to-model comparison, the 20C3M monthly rainfall, winds, and SST datasets for the period from 1970 to 1999 were collected from the Coupled Model Intercomparison Project phase 3 (CMIP3). Table 1 summarizes the models. Note that only the first realization of each model was analyzed to preserve the interannual signal. The model outputs were, then, remapped onto a common grid system of 2.5° × 2.5° for fair intercomparison by conducting bilinear interpolation.

3. Global monsoon climatology

a. Annual mean and annual cycles

Wang and Ding (2008) extracted the major modes of seasonal variability in global precipitation and circulations through the application of a multivariate empirical orthogonal function (MVEOF) to the climatological annual cycle of precipitation and 850-hPa winds. The results showed that the first two leading modes together account for ~84% of the total annual variance of the climatological annual cycle of global precipitation and low-level winds with the maximum and minimum of the first (second) mode occurring around local summer (spring) and winter (fall). They further showed that the spatial patterns of the first and second modes can be faithfully represented by June–September minus December–March mean (AC1) and April–May minus October–November mean (AC2).

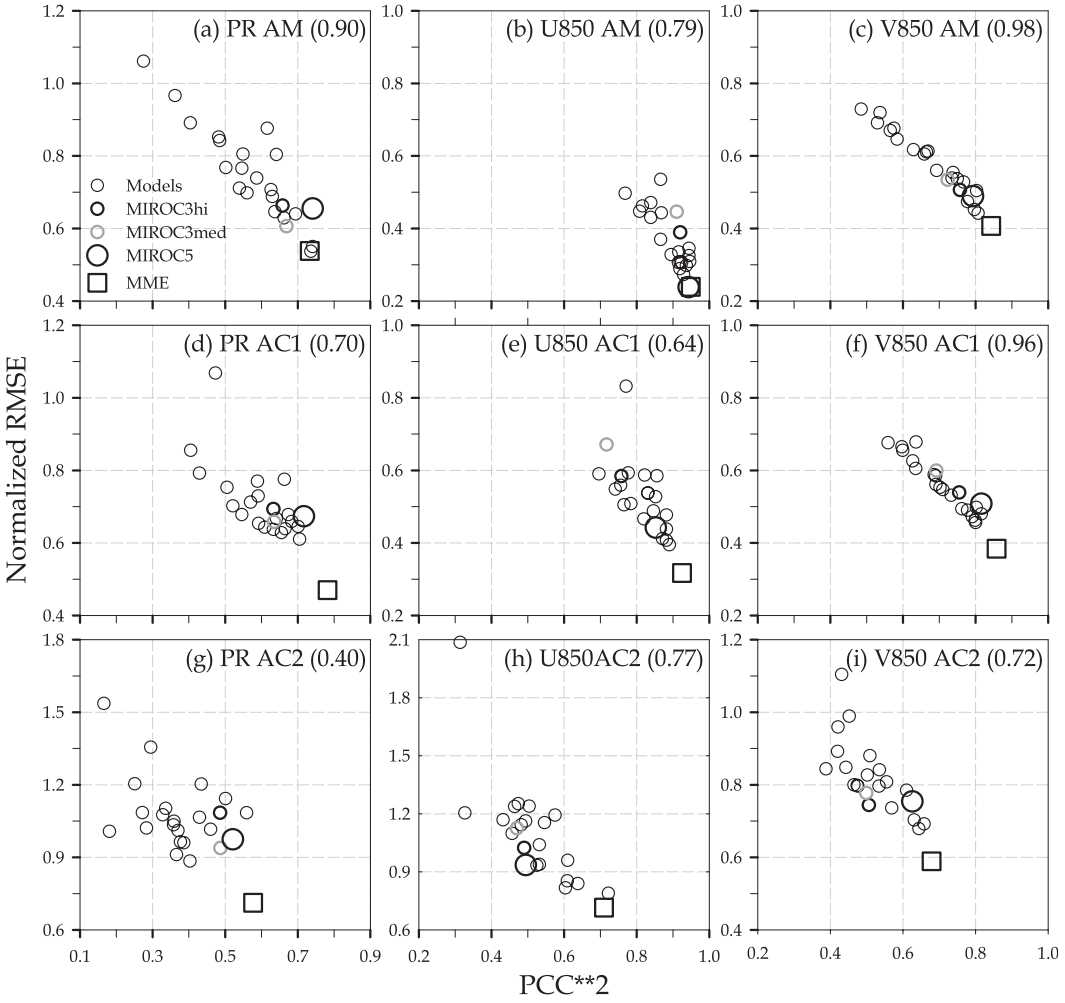

FIG. 1. Evaluation of the CGCM performances on the annual climatology of (left) precipitation and (middle) zonal and (right) meridional 850 hPa wind. The abscissa (ordinate) is the pattern correlation coefficient (PCC) squared (domain-averaged RMSE normalized by the observed spatial standard deviation); numbers in parenthesis indicate linear regression coefficients. Domain used is 40°S–45°N, 0°–360°E.

To assess the performance of MIROC5 in modeling climatological annual variation, we first examine the annual mean (AM), AC1, and AC2 in comparison with the two versions of MIROC3, the CMIP3 CGCMs, and the multimodel ensemble (MME) mean, derived from the simple arithmetic average among the CMIP3 models.

Figure 1 compares multimodel performances on the AM, AC1, and AC2 of precipitation and 850-hPa zonal and meridional winds in terms of the coefficient of determination (in other words, square of the Pearson pattern correlation coefficient γ^2) and domain-averaged rms error (RMSE) normalized by the observed spatial standard deviation over the global tropics and subtropics (40°S–45°N, 0°–360°E). First, it is noted that the γ^2 and RMSE for the CMIP3 model outputs have a statistically significant linear relationship with confidence level higher than 95% (regression coefficient is given in parenthesis). The PR AC2 (Fig. 1g) is only one outlier of such linearity. Thus, a model with a higher γ^2 tends to have a smaller RMSE. Second, the γ^2 (RMSE) is lowest (largest) in the AC2, suggesting that the current CGCMs have difficulty in representing premonsoon and/or postmonsoon conditions. Third, for the square of the pattern correlation coefficients (PCCs) of all annual components, MIROC5 unexceptionally outperforms MIROC3 and is generally superior to the CMIP3 models. Besides, its biases are, when compared with MIROC3, either reduced in wind fields or, at least, not degraded in precipitation.

b. Global monsoon precipitation and circulations

The annual evolution of the first two leading MVEOF modes reflects the seasonal contrast between rainy summer

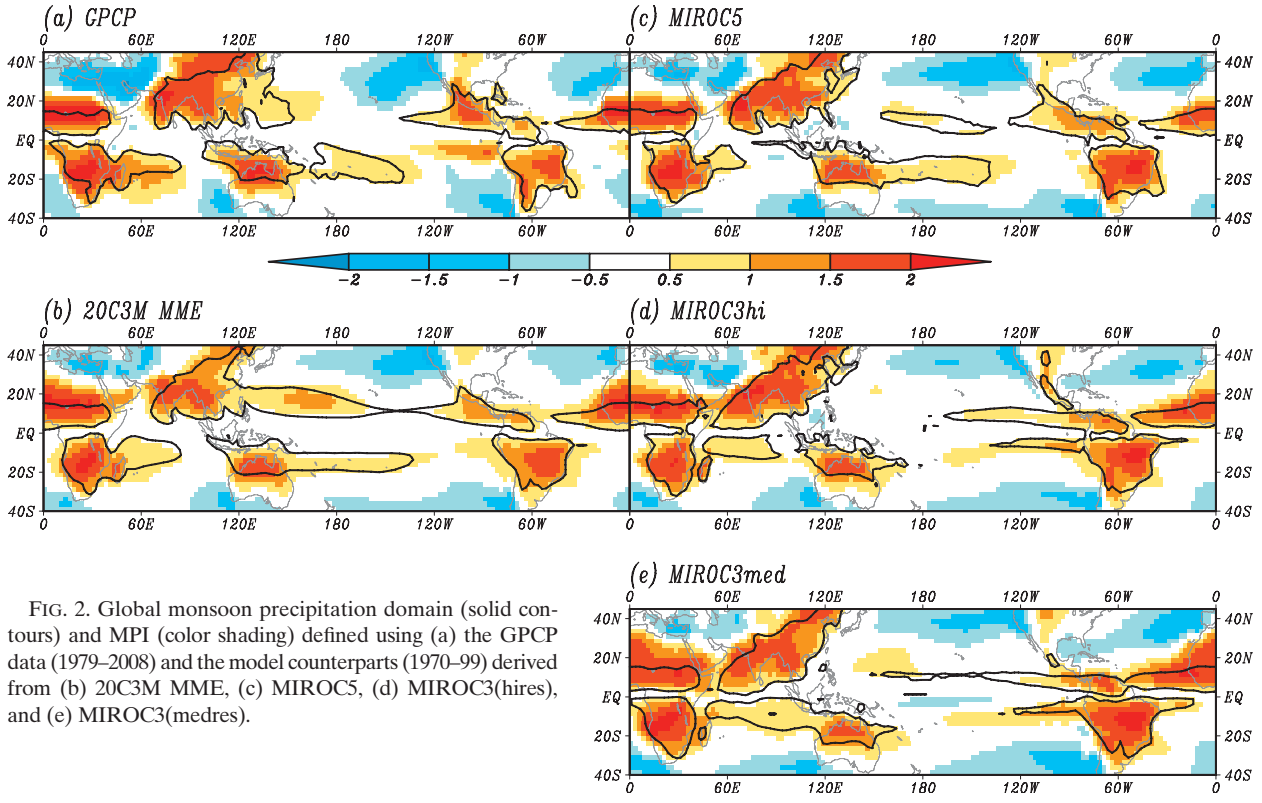

FIG. 2. Global monsoon precipitation domain (solid contours) and MPI (color shading) defined using (a) the GPCP data (1979–2008) and the model counterparts (1970–99) derived from (b) 20C3M MME, (c) MIROC5, (d) MIROC3(hires), and (e) MIROC3(medres).

and dry winter as well as the seasonal reversal of low-level winds. Because the monsoon climate features these characteristics, Wang et al. (2011a) delineated the global monsoon precipitation domain as the annual range (AR) of precipitation rate exceeding a threshold of 2.5 mm day^{-1}, where

$$\mathrm{AR} = \text{MJJAS (NDJFM) minus NDJFM (MJJAS) in NH (SH)},$$

where MJJAS (NDJFM) indicates the May–September (November–March) mean precipitation rate in the Northern (NH) and Southern (SH) Hemisphere. Note that the AR is defined by the combination of the first two leading MVEOF modes. The AR could be used to measure the monsoon precipitation intensity. However, because of its latitudinal dependency, an alternative measure, monsoon preicipitation index (MPI), is defined as

$$\mathrm{MPI} \equiv \mathrm{AR/AM}.$$

Similarly, the monsoon circulation domain can be demarcated as the AR of the westerly winds or poleward winds at 850 hPa exceeds 2.5 m s^{-1}. This threshold value is also chosen carefully to be consistent with the criteria used in Wang and Ding (2008). The monsoon circulation index (MCI), a measure for monsoon circulation intensity, is defined in the same way as for MPI except using wind speed to utilize both zonal and meridional winds in an integrated manner. The use of wind speed, however, makes it difficult to distinguish the tropical MCI with positive zonal wind AR from the extratropical MCI with negative zonal wind AR. Thus, the final MCI is derived by multiplying the sign of zonal wind AR to the AR/AM ratio of wind speed.

Figure 2 shows the observed and simulated monsoon precipitation domain (solid curves) and index (shadings). It is apparent from the observation that the use of the simple criterion separates the monsoon precipitation regime quite well from the dry, Mediterranean, and equatorial perennial rainfall regimes. The global monsoon precipitation domain consists of six major monsoon regions: Southeast Asia, Indonesia–Australia, North and South Africa, and North and South America. All of these major monsoon regions encompass adjacent marginal seas and oceanic regions, which signifies a land–sea thermal contrast. Thus, the oceanic monsoon is an essential component of a regional monsoon. In the subtropical mid South Pacific, on the other hand, there is a pure oceanic region that does not involve land–sea thermal contrast but follows the typical seasonal distribution of monsoon precipitation. Therefore, this region is ruled out from the monsoon precipitation

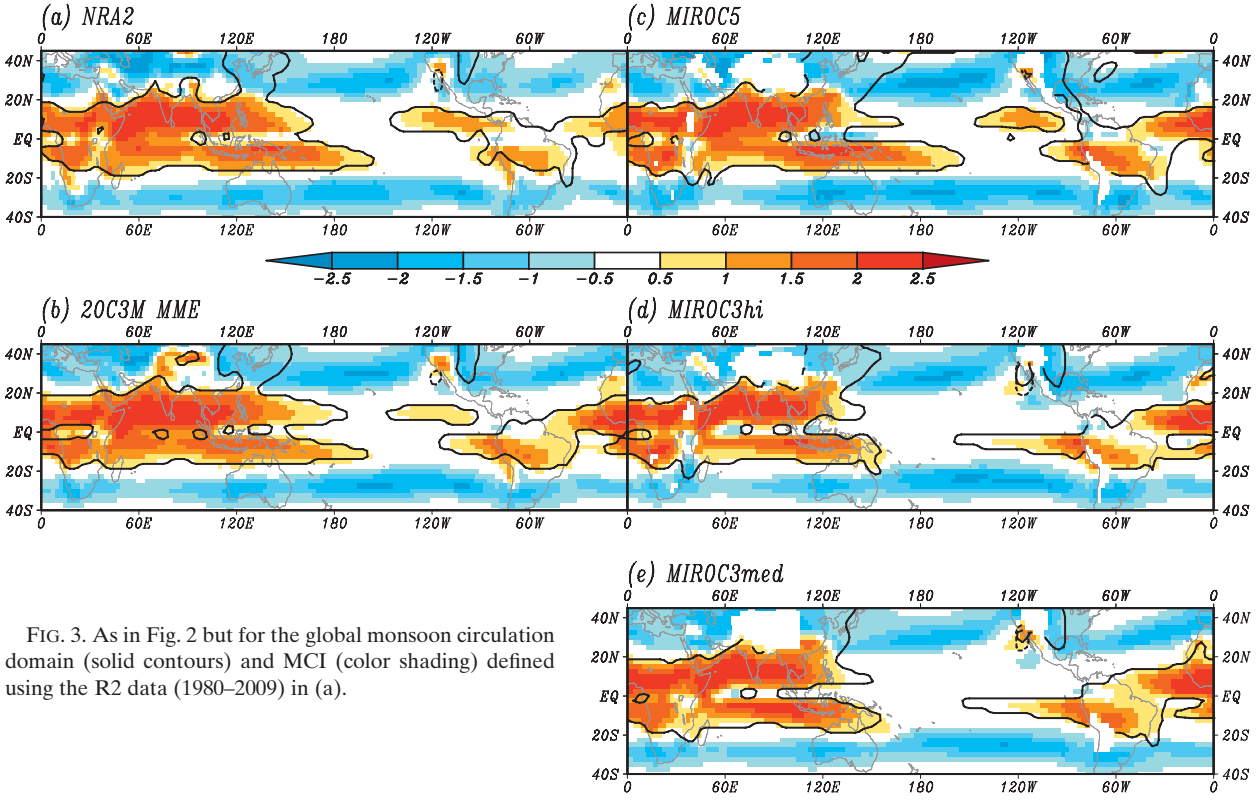

FIG. 3. As in Fig. 2 but for the global monsoon circulation domain (solid contours) and MCI (color shading) defined using the R2 data (1980–2009) in (a).

domain. It should be also mentioned that there are some regions, for instance, tropical Southeast Asia, where both local summer and winter monsoons appear to be equally important (Chang et al. 2005). However, the suggested regions are narrowly confined to the north of the equator. More notably, the seasonal rainfall contrast of the local winter monsoon is far weaker than that of the local summer monsoon: none of the local winter monsoon regions suggested in Chang et al. (2005) passes the threshold seasonality of 2.5 mm day^{-1} (figure not shown). This indicates that, even though the local summer and winter monsoons coexist in the same hemisphere, the local summer monsoon is the typical event after all.

Globally, the monsoon precipitation domains modeled by the MIROC versions are in general agreement with the observed (Figs. 2c–e). Regional details, however, differ remarkably between MIROC5 and MIROC3. For the South Asian monsoon, for example, MIROC5 compares quite favorably with observations on the southeastern coast of the Indian subcontinent. The North American monsoon domain is also reproduced better in MIROC5 than in MIROC3. Note that not only MIROC3(medres) but also MIROC3(hires), which has the finest spatial resolution among the MIROCs, failed to reproduce such regional details in the aforementioned domains. Common errors also exist among the MIROC versions as revealed by the absence of monsoon domains over the western North Pacific. Further investigation shows that the source of errors is attributable to the underestimation of MJJAS precipitation and overestimation of NDJFM precipitation. Some of the CMIP3 models seem to be able to replicate the western North Pacific monsoon domains, as inferred from Fig. 2b.

Figure 3 presents the global monsoon circulation domains and index in the same format with Fig. 2. The observed Eastern Hemispheric tropical monsoon circulation domains that are symmetric and straddling the equator are depicted by the seasonal reversal of zonal winds. Meanwhile, the criterion of poleward winds allows us to pick up the East Asian monsoon regions. The North American monsoons are demarcated by zonal winds with the threshold being relaxed to 1.5 m s^{-1} due to the weak amplitude of wind reversal (dashed curves). The South American monsoon circulation domains are portrayed by both zonal and poleward wind criteria. These monsoon circulation domains are physically consistent with the monsoon precipitation domains as discussed in Wang and Ding (2008). All of the MIROC simulations are able to reproduce the monsoon circulation domains through the corresponding wind criteria. Yet differences are seen over the tropical eastern Pacific. While MIROC5 can reproduce the monsoon domains north of the equator,

those in MIROC3 seem to be shifted far southward and eventually merged with the South American branch. Again, these errors appear to be model-dependent since the CMIP3 multimodle ensemble bears close resemblance to the observation over the tropical eastern Pacific.

The panels in Fig. 4 summarize the multimodel performance in simulating global monsoon intensity (Fig. 4a) and domain (Fig. 4b). Here, we take advantage of the threat score (TS) (Wilks 1995) to assess model reproducibility on global monsoon domains. The TS is defined as the ratio of "hit" grids to the sum of hit, missed, and false-alarm grids. The hit grid indicates the grid at which model and observation match each other, and the missed grid means an observed grid being missed in the simulation, and the false-alarm grid is a grid that is recognized solely by the model. The TS ranges from 0 to 1 with 0 being the worst agreement between the observation and simulation. The performance of the CMIP3 models shows a linear relationship between monsoon precipitation and circulation with a regression coefficient of 0.53 and 0.80 for intensity and domain, respectively. The linearity of global monsoon intensity becomes stronger (0.71) if the two exceptions located at middle left were excluded. All of these relations are significant at a confidence level higher than 99%. A comparison among MIROC simulations demonstrates the importance of the physical parameterization. Though the intensity and domain of global monsoon precipitation are improved for a higher resolution, those of global monsoon circulation are ameliorated little [MIROC3(medres) vs MIROC3(hires)]. In contrast, the improved physical schemes lead to better representation not only for the monsoon precipitation but also for the monsoon circulation (two MIROC3s vs MIROC5). It is recognized further that the low-level winds are reproduced better than precipitation both in terms of intensity and domain, which is also generally valid among the CMIP3 models. Such superiority of the large-scale dynamical fluctuation to the rainfall variation has been reported on the interannual time scale as well (Sperber and Palmer 1996; Sperber et al. 1999). One possible explanation is that even though the modeled precipitation occurs at slightly different places from the observed, the response of the geostrophic winds would not deviate substantially from the observations as long as the precipitation events lie in common within the Rossby radius of deformation.

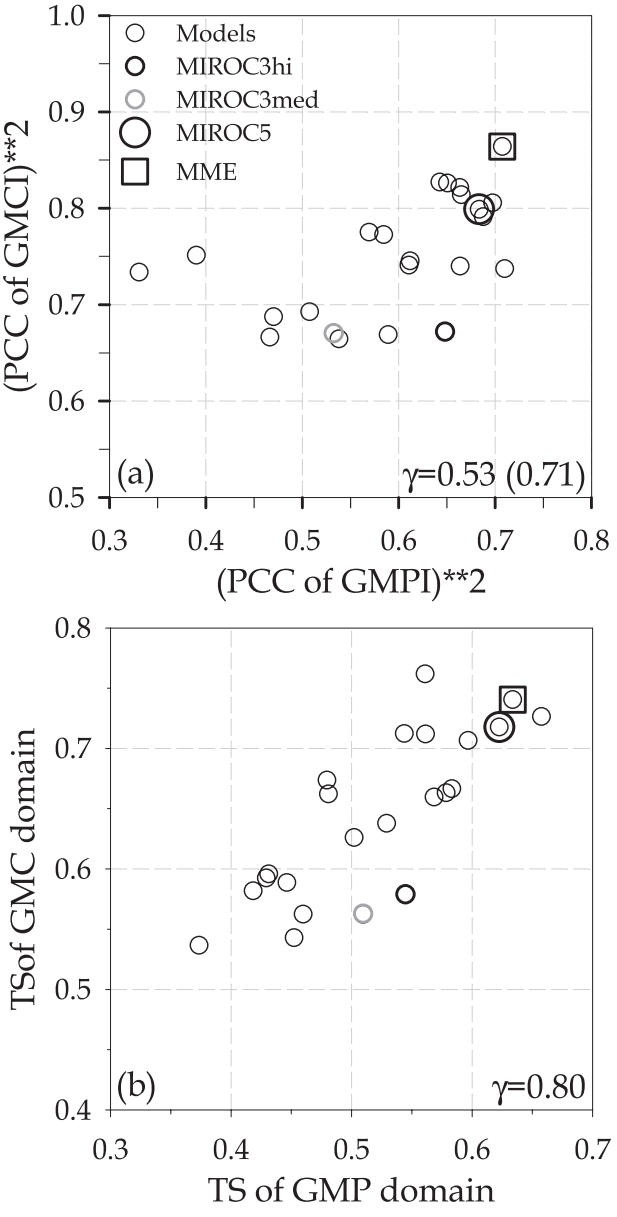

FIG. 4. Evaluation of the CGCM performance on (a) the climatological global monsoon index and (b) domain. In (a) the abscissa (ordinate) is the PCC squared of the global MPI (global MCI), and in (b) the threat score is plotted for the global monsoon precipitation (GMP) domain (abscissa) vs global monsoon circulation (GMC) domain (ordinate). The regression coefficient is shown in lower-right corner of each panel. Domain used is 40°S–45°N, 0°–360°E.

4. El Niño properties: Amplitude, asymmetricity, and periodicity

As mentioned earlier, MIROC3 is unable to reproduce sufficiently the amplitude of El Niño although the zonal gradient of the mean thermocline is realistic (Guilyardi et al. 2009). This is evident in Fig. 5a, which compares the observed and modeled El Niño amplitude measured by the standard deviation (SD) of the monthly Niño-3 index, that is, area-averaged (5°S–5°N, 90°–150°W) monthly SST anomaly calculated by removing the climatological monthly mean. The El Niño amplitude in

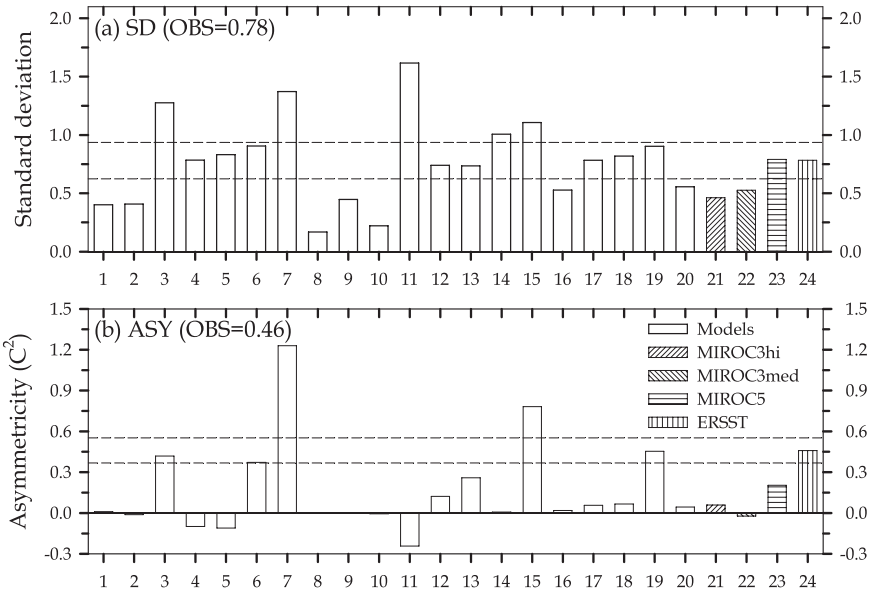

FIG. 5. (a) Standard deviation and (b) asymmetricity of the monthly Niño-3 index: the dashed line denotes the ±20% limits of the observed value.

MIROC3 is underestimated by about 35%. In contrast, the SD of MIROC5 is nearly the same as the observed. The amplitude of CMIP3 CGCMs varies widely from one model to another. Nevertheless, about one-third of the models are able to replicate a reasonably realistic El Niño amplitude.

Another useful measure for El Niño reproducibility is skewness. Several previous studies (Jin et al. 2003; An and Jin 2004; An et al. 2005) have measured the observed El Niño nonlinearity over the equatorial Pacific through a statistical method (skweness). They pointed out that El Niño has strong nonlinearity that causes the asymmetry of El Niño, with El Niño being stronger than La Niña. The skewness by definition is a measure of the asymmetry of a probability distribution function and is zero for a normal distribution (White 1980). It is defined as the normalized third statistical moment $[m_3/(m_2)^{3/2}]$, where m_k is the kth moment,

$$m_k = \sum_{i=1}^{N} (x_i - \overline{X})^k / N,$$

in which x_i is the ith observation, $\overline{X}$ is the mean, and N is the number of observations. The original definition, however, can cause a large skewness when the standard deviation is less than a unit. Thus, to avoid such difficulty, the asymmetricity, defined as $m_3/(m_2)^{1/2}$ (An et al. 2005), is used in the present study. The statistical significance of the asymmetricity can be estimated from the standard error of asymmetricity (White 1980). In nature, the asymmetricity is significantly positive near the east coast of the South American continent and tends to decrease to the west (e.g., An et al. 2005). As a result, the asymmetricity of the monthly Niño-3 index that is an area average over the equatorial eastern Pacific seldom passes the significant test. Thus, asymmetricity greater than observed will be subjectively considered significant. The asymmetricity of the monthly Niño-3 index obtained from the observation and model simulations is presented in Fig. 5b. The majority of the CMIP3 CGCMs, including the two versions of MIROC3, have a very small asymmetricity, hence similar to the normal distribution. Several models are negatively skewed, inferring that cold events are unrealistically stronger than warm events. Only three models have a positive asymmetricity as large as that observed. For the MIROC5 simulation, the asymmetricity is positive but the amplitude is about half of the observed. Interestingly, the models with a large positive skewness have intensified amplitude without exception (Figs. 5a and 5b). Therefore, it is argued that nonlinearity likely necessitates sufficient amplitude.

The dominant periods of the monthly Niño-3 index that pass the red noise test with 95% confidence level are plotted in Fig. 6. The observation exhibits a clear separation between high and low frequency variability. They represent the annual-to-quasi-biennial mode ($1 \leq$ period < 2.5 yr) and the El Niño mode ($3 \leq$ period < 5 yr). Only one CMIP3 CGCM can capture such separation of

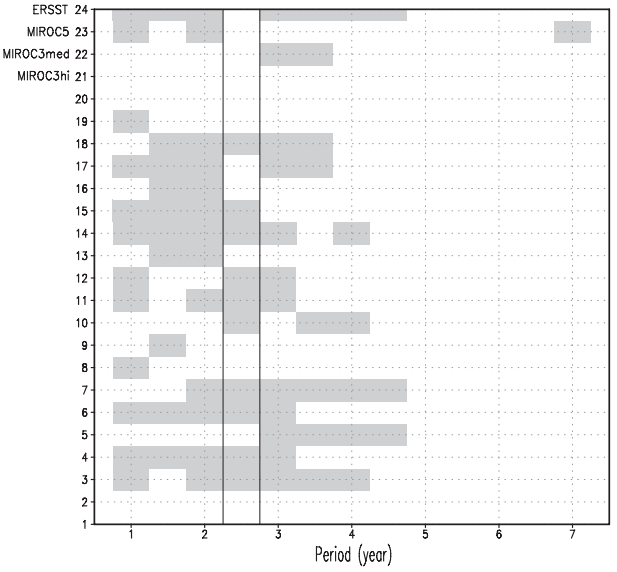

FIG. 6. Dominant periods of the monthly Niño-3 index: periods that pass the red noise test at the 95% confidence level.

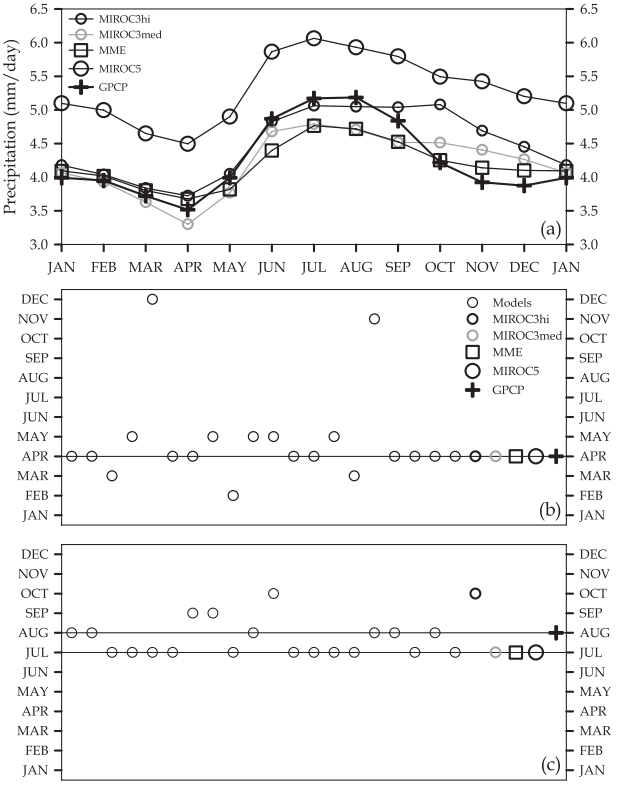

FIG. 7. (a) Climatological annual cycle of precipitation averaged over the observed global monsoon domain. Scatter diagrams for the month of the (b) minimum and (c) maximum precipitation. The domain used is 40°S–45°N, 0°–360°E.

periodicity. Several models, including MIROC3(hires) are not able to reproduce both modes. The rest of the models, including MIROC3(medres), are only partially successful at capturing the observed variability. Recently, Lin (2007) examined the interdecadal variability of ENSO in the CMIP3 CGCMs and argued that MIROC3(medres) has substantial variance distributed at a period longer than 6 yr without conducting a significant test. Our analysis also shows a similar periodicity in the MIROC3(medres) outputs. However, the power spectrum for the low frequency variability does not pass the 95% confidence level (figure not shown). This low frequency variability becomes significant in MIROC5 in which the high frequency variability is also reproduced to some degree.

5. Interannual variability of ENSO–global monsoon precipitation

a. Observation and multimodel simulations

Conventional efforts devoted to the study of interannual monsoon variability have usually shed light on the regional aspects of each monsoon system due to its indigenous characteristics. Wang et al. (2011b, manuscript submitted to *Nat. Geosci.*), however, recently demonstrated that, by means of the global monsoon concept used in the present study, all regional monsoons can be viewed as an integrated system. In this section, we adopt their methodology to evaluate the realism of the simulated interannual global monsoon variability with particular focus on the coherent patterns with low- and midlatitude SST.

Investigation of year-to-year variability is usually based on the calendar-year average. This approach is, however, inappropriate at least in terms of global monsoon precipitation (Wang et al. 2011b, manuscript submitted to *Nat. Geosci.*). Figure 7a illustrates the climatological annual cycle of precipitation over the global monsoon domain. The observation has a primary peak in July–August and a secondary peak in January–February owing to the NH and SH monsoons. Also a prominent minimum takes place in April. These seasonal variations are robust in other observation datasets too [e.g. the Climate Prediction Center (CPC) Merged Analysis of Precipitation (CMAP) (Xie and Arkin 1997) and Precipitation Reconstruction over Land (PREC/L) (Chen et al. 2002)]. As such, the "monsoon year," spanning from May to the subsequent April, is used in the present study to investigate the interannual variability of global monsoon precipitation. Figures 7b and 7c summarize the month of primary valley and peak obtained from the model simulations. Here, the GPCP global monsoon domain is used in common for all models. Most of the CMIP3 models are able to pick up the

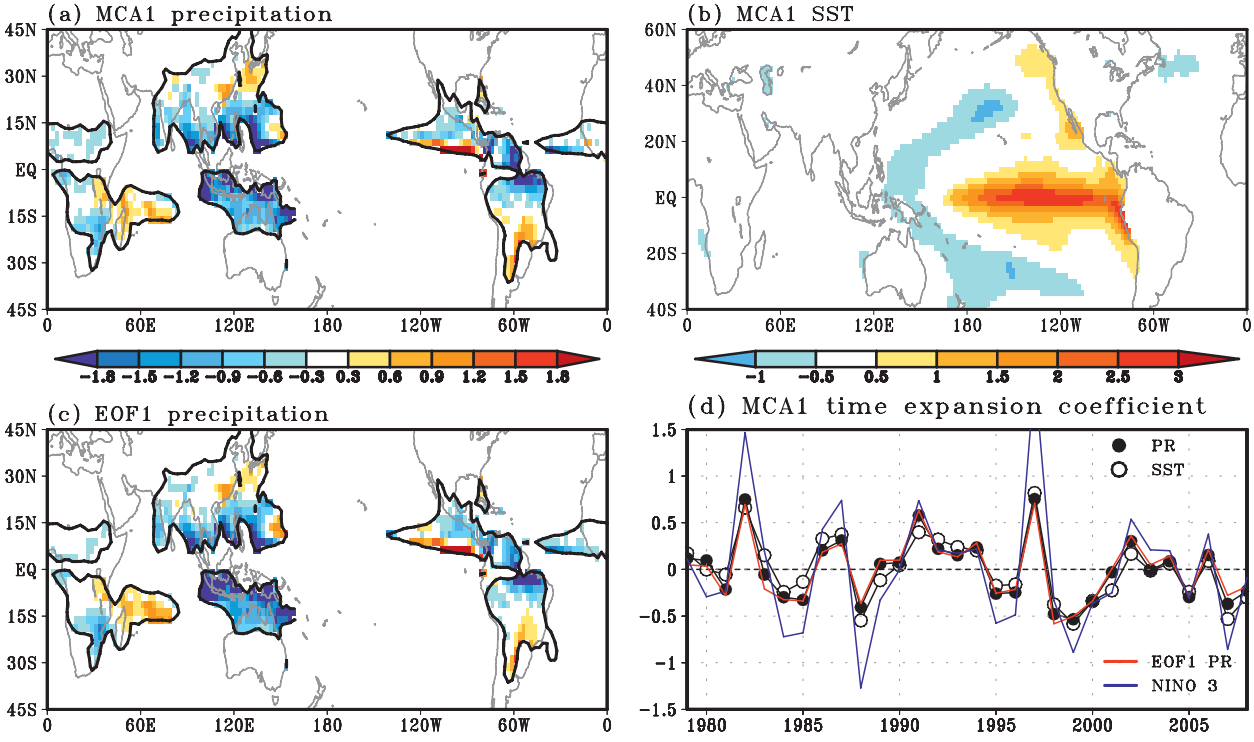

FIG. 8. The leading mode of monsoon precipitation and SST obtained from the MCA and EOF analyses: the spatial patterns of (a) global monsoon precipitation and (b) SST obtained from the MCA, (c) global monsoon precipitation obtained from the EOF, and (d) corresponding time expansion coefficients. For comparison, the Niño-3 SST anomaly averaged over the monsoon year is shown in (d). Data period is 1979–2008.

primary peak in July–August. Meanwhile, the April minimum is missed in half of the CGCMs. The two versions of MIROC3 reproduce the April valley with a realistic magnitude. But MIROC3(hires) tends to overpredict monsoon precipitation from September to December (also see Fig. 7a) and, as a result, the major peak occurs in October. In MIROC5, this caveat is remedied. In addition, the seasonal evolution of the annual cycle is akin to the observed. However, the magnitude of the annual cycle is systematically overestimated by about 25% year-round. The cumulus parameterization in MIROC5 was newly introduced by Chikira and Sugiyama (2010). The replacement led to a very realistic representation of precipitation patterns over the tropics and subtropics (Chikira 2010). Nonetheless, shortcomings appeared to be heavy rainfall over South Africa, the Indian subcontinent, southern China, the Maritime Continent, and Brazil (Watanabe et al. 2010), all of which fall into the global monsoon precipitation domains, thereby contributing to overprediction.

Figure 8 shows the first leading MCA mode between rainfall within the global monsoon precipitation domain [precipitation rate (PR) MCA1 (Fig. 8a)] and SST over the global tropics and extratropics (SST MCA1; Fig. 8b) and corresponding time expansion coefficients (Fig. 8d) obtained from the observations. The MCA1 accounts for about two-thirds of the total covariance, and the temporal correlation between the PR MCA1 and SST MCA1 is 0.94. Of note is that the spatial patterns of the SST MCA1 exhibit a warm phase of ENSO over the tropical Pacific and its time coefficient is nearly identical to the time series of the monsoon-year mean Niño-3 SST anomaly. The MCA1, therefore, illustrates the interannual rainfall variability over the global monsoon domain that is coupled with El Niño variability. The footprints of El Niño in rainfall distribution appeared as the negative anomalies over the majority of the monsoon domain and the scattered positive anomalies in the Southern Hemisphere monsoon domain. The increased (decreased) rainfall result from El Niño (La Niña). It has been known that during the development (boreal summer) and mature phases (austral summer) of El Niño events, the warmer SST in the eastern central Pacific shifts the equatorial Pacific rainbands (i.e., the intertropical convergence zone and the South Pacific convergence zone) equatorward, thereby directly suppressing Asian–Australian and North American monsoon rainfall. The mature phase of El Niño also diminishes rainfall over continental South Africa and northern South America through atmospheric teleconnections.

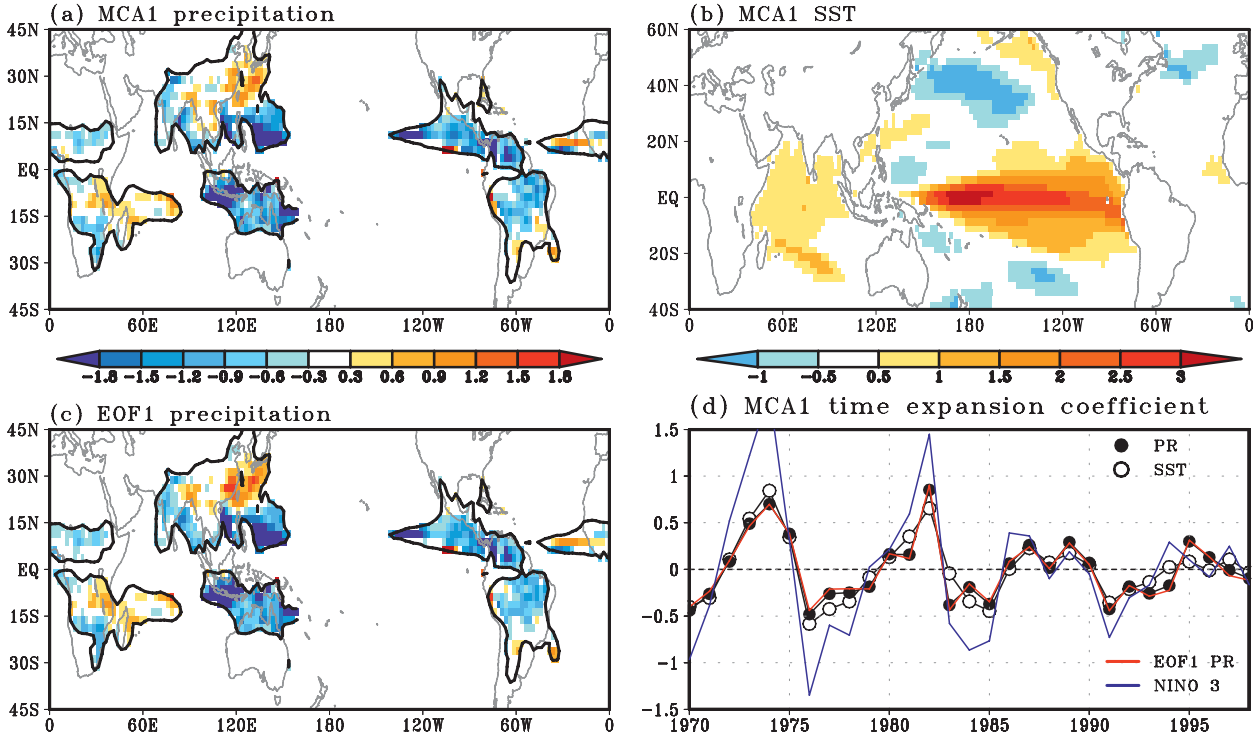

FIG. 9. As in Fig. 8 but for the MIROC5 simulations over 1970–98.

Now a question arises as to whether these precipitation patterns that are concatenated with El Niño are also visible in the year-to-year global monsoon precipitation variability. To answer this question, we applied the EOF analysis to the global monsoon precipitation itself: the first leading EOF mode (PR EOF1) is presented in Figs. 8c and 8d. Interestingly, the spatiotemporal patterns of the PR EOF1, which explain about 24% of the total variance, agree extremely well with the PR MCA1 with pattern and temporal correlation coefficients of 0.96 and 0.99, respectively. Thus, it can be suggested that El Niño plays a pivotal role in determining the interannual variability of the global monsoon precipitation.

How well does the year-to-year coupling work in the CGCMs? It is found in the MIROC5 simulation that El Niño also greatly affects global monsoon precipitation (Fig. 9). The MCA1 explains about 81% of the total covariance, and the temporal correlation between rainfall and SST is 0.90. The SST MCA1 exhibits the El Niño patterns seen in the observation, and the time coefficients are in tandem with the time series of the Niño-3 index. The PR EOF1 accounts for about 21% of the total variance, and its spatiotemporal patterns are virtually identical to the PR MCA1 with correlation coefficients greater than 0.98 for both time and space. The impacts of El Niño are also of vital importance across the CMIP3 models: 19 (12) out of the 22 models that have El Niño amplitude greater than 50% (80%) of the observed show a PCC between PR EOF1 and PR MCA1 higher than 0.66 (0.80) (figure not shown).

The aforementioned results suggest a clear link between SST anomalies in the equatorial Pacific and rainfall anomalies over the global monsoon domain. Thus, one may plausibly assume that improved El Niño simulation entails more realistic monsoon precipitation in a model. To test this hypothesis, a scatter diagram of spatial similarity between the observation and model simulations is presented (Fig. 10). The skill of global monsoon variability (PCC for PR EOF1, ordinate) is linearly related to that of tropical SST variability (PCC for SST MCA1, abscissa) with a regression coefficient of 0.51 (0.69 without one outlier at middle left) that is statistically significant at the 99% confidence level. Thus, the fidelity of the global monsoon rainfall indeed depends upon the reality of the tropical SST. For the MIROC simulations, for instance, the PCCs between the simulated and observed SST MCA1 are increased from MIROC3 [0.68 for MIROC3(hires) and 0.70 for MIROC3(medres)] to MIROC5 (0.84). As a consequence, the PR EOF1 simulation of MIROC5 is improved remarkably to a PCC of 0.56 compared with that of the two MIROC3 versions, of which PCCs are below 0.25. Note also that applying an enhanced resolution does not result in an

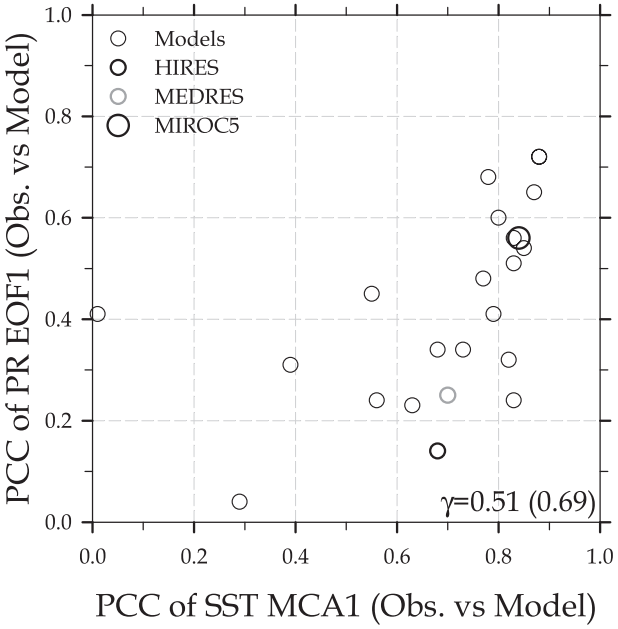

FIG. 10. Evaluation of CGCM performance on the spatial similarity of tropical SST and global monsoon precipitation: abscissa (ordinate) is the PCC of SST MCA1 (PR EOF1). The regression coefficient is shown in the lower-right corner.

appreciable difference between MIROC3(medres) and MIROC3(hires). These results once again reflect the importance of the advanced physical parameterization in a model.

b. *Possible mechanism for the improved simulation of ENSO in MIROC5*

On an interannual time scale, the classical feedback described by Bjerknes (1969) is generally believed to regulate the state of the tropical Pacific and amplify incipient El Niño events (e.g., Collins et al. 2010). Thus, in search of the underlying mechanism that is possibly responsible for the MIROC5 improvement in El Niño simulation, further analyses are made with particular focus on the Walker circulation in the Pacific as this zonally aligned overturning circulation is a key player not only for the initiation but also for the intensification of the positive feedback loop. Climatologically, the upward motion of the Walker circulation along the equatorial plane is placed over the western Pacific and Maritime Continents, with a maximum over Indonesia (115°–120°E) (Lau and Yang 2003). However, during El Niño, strong updraft prevails over the equatorial central Pacific, which induces a less-vigorous Walker circulation and hence intensifies the Bjerknes feedback. Here, we use precipitation averaged over 5°S–5°N, 115°–120°E (160°–200°E) as a proxy for the rising limb of the Pacific Walker circulation (ascending motion due to El Niño) as this overturning circulation is basically driven by the diabatic heating processes (via the release of latent heat in the atmosphere) in connection with the divergent component of the tropical winds.

Figure 11a shows lead–lag correlation coefficients of the monthly precipitation anomalies averaged over the maximum upward branch of the climatological Walker circulation with respect to the monthly Niño-3 index. Note that the 3-month running average was applied prior to calculation. The decorrelation time for such smoothed time series is 9–10 months (figure not shown). Thus, the effective degree of freedom is estimated as 360/9.5 and a correlation of ±0.31 reaches the 95% significance level based on a t test. In observation, the rising motion of the Walker circulation is generally negatively correlated with the Niño-3 index over a wide range of lead–lag times, with maximum correlation when the former leads by 1–2 months. The observed convective activity in response to anomalous SST warming is displayed in Fig. 11b. Large positive rainfall anomalies are accompanied mostly by positive SST anomalies, indicating that the warmth of the SST is of importance for deep convection to occur. The implication of these results is that El Niño events are often triggered by slowing down the Walker circulation at a rising branch and, once established, the convective activity over the central Pacific is a key to the amplification of the Bjerknes feedback. Obviously, the two versions of MIROC3 are less skillful mimicking the initiation and intensification of the feedback loop; the correlation coefficients are insignificant at all lead–lag ranges (Fig. 11a), and there is no sign of strong convection, albeit the SST anomalies often reach up to 2°C (Figs. 11d and 11e). In MIROC5, in comparison, the Bjerknes feedback appears to play a nontrivial role. The suppressed Walker circulation in association with the reduction of precipitation seems to be able to excite El Niño events with a reasonable realistic lead time (Fig. 11a). Furthermore, enhanced deep convection tend to occur more frequently in proximity of the 2°C warming of SST (Fig. 11c).

6. Concluding remarks

By using process- and feedback-based metrics, the present study casts light on the fidelity of the prime examples of the forced response (global monsoon), internal feedback process (El Niño), and their year-to-year coupling simulated by the new model version, MIROC5, in comparison with its predecessor having coarser and finer resolutions than MIROC5 [MIROC3(medres) and MIROC3(hires), respectively] and the coupled global climate models participating in the CMIP3. The effect

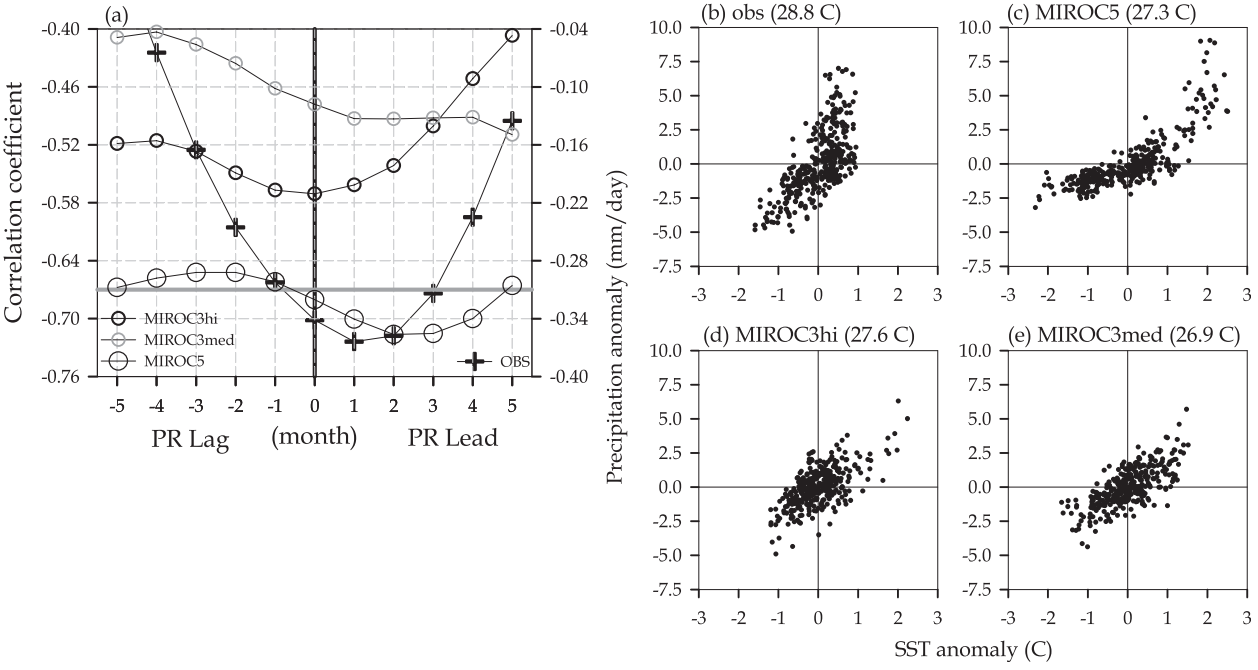

FIG. 11. (a) Lead–lag correlation coefficients of the monthly precipitation anomalies averaged over the maximum upward branch of the climatological Walker circulation (5°S–5°N, 115°–120°E) with respect to the monthly Niño-3 index obtained from the observations (scale on the left) and MIROC simulations (scale on the right). Note that a 3-month running average is applied prior to calculation. Horizontal gray line denotes the 95% confidence level with scale on the right. Scatterplots of monthly SST and precipitation averaged over the equatorial central Pacific (5°S–5°N, 160°–200°E) for (b) observation, (c) MIROC5, (d) MIROC3(hires), and (e) MIROC3(medres). Numbers in parenthesis indicate climatological mean SST averaged over the analysis domain.

of El Niño on regional monsoons has long been a topic of interest. In contrast, its influence on the global monsoon as a whole has received little attention and, hence, was investigated in the present study. Thirty years of observational data and the Twentieth-Century Climate in the Coupled Model simulations are analyzed using a set of diagnostic metrics and the maximum covariance analysis to assess the reality of monsoon climatology and the interannual El Niño–monsoon relationship, respectively.

MIROC3(hires), the model with the highest resolution, reproduces better the domain and intensity of global monsoon precipitation when compared with MIROC3(medres), the model with the lowest resolution and sharing the same physical schemes with MIROC3(hires). On the other hand, MIROC5, the model with moderate resolution but improved parameterizations, considerably outperforms the two versions of MIROC3 and is generally superior to the CMIP3 models in simulating global monsoon precipitation as well as the circulation. This is the result of overall improvement in the climatology of the annual mean and the two components of the annual cycle. Furthermore, the simulation of the year-to-year variability of global monsoon precipitation is improved substantially from MIROC3 to MIROC5. These are suggestive of the importance of continuously developing physical processes in a model.

Unlike observations, most CMIP3 CGCMs exhibit normally distributed El Niño, with SST asymmetricity near zero in the tropical Pacific. The reality of the El Niño nonlinearity also remains unsatisfactory from MIROC3 to MIROC5. In the latter, however, the amplitude and periodicity of El Niño are improved to some degree.

As recently pointed out by Wang et al. (2011b, manuscript submitted to *Nat. Geosci.*), the MCA shows observational evidence of the salient year-to-year interplay between El Niño and global monsoon precipitation. Multimodel results indicate that such linkage is robust across the contemporary CGCMs and the reality of the spatial patterns of global monsoon rainfall significantly depends upon the reproducibility of the tropical SST distributions. In particular, MIROC5 simulates the spatial patterns of the interannual tropical SST swing quite realistically as compared with the old versions, which entails an improved simulation of interannual global monsoon precipitation. Better representation of El Niño and its teleconnection with global monsoon precipitation is likely ascribed to the newly incorporated cumulus convection scheme, which enables MIROC5

to mimic the Bjerknes feedback loop to some extent through strengthening of the convective activity over the equatorial central Pacific. The intensified convection is able to improve further the positive feedback process: Watanabe et al. (2011) showed that the Bjerknes feedback in MIROC5 tends to be more effective if the deep convection along the eastern ITCZ is enhanced through reduction of the entrainment rate.

The better reproducibility of MIROC5 bodes well for its use in future climate projection. Though CGCMs have been extensively used to predict future climate changes, assessing the accuracy of the model projection is hampered owing to limited knowledge of the highly complex climate system. Thus, the fidelity of a CGCM's performance for current climate variations is alternatively considered a measure of its capability to project the future (Kim et al. 2008). In this context, near-term to century-long predictions of MIROC5, which are currently being undertaken, would be more reliable. Specifically, the forthcoming international collaboration, such as CMIP5, calls for intergraded efforts from around the world to meet the needs of both the scientific community and the public. The results suggest that MIROC5 will be able to contribute to such efforts as a credible member.

Acknowledgments. We thank the anonymous reviewers for valuable suggestions. We also acknowledge the modeling groups for making their simulations available for analysis, the Program for Climate Model Diagnosis and Intercomparison (PCMDI) for collecting and archiving the CMIP3 model output, and the WCRP's Working Group on Coupled Modelling (WGCM) for organizing the model data analysis activity. The WCRP CMIP3 multimodel dataset is supported by the Office of Science, U.S. Department of Energy. This work was performed under the auspices of the Ministry of the Environment, Japan, under the Environment Research & Technology Development Fund (Grant A0902). MW, MK, and TY were supported by the Innovative Program of Climate Change Projection for the 21st Century (Kakushin Program) of the Ministry of Education, Culture, Sports, Science and Technology, Japan. BW was supported by APEC Climate Center. The computation was carried out on the Earth Simulator.

REFERENCES

AchutaRao, K. M., and K. R. Sperber, 2006: ENSO simulation in coupled ocean-atmosphere models: Are the current models better? *Climate Dyn.,* **27,** 1–15.

Adler, R. F., and Coauthors, 2003: The Version-2 Global Precipitation Climatology Project (GPCP) monthly precipitation analysis (1979–present). *J. Hydrometeor.,* **4,** 1147–1167.

An, S.-I., and F. F. Jin, 2004: Nonlinearity and asymmetry of ENSO. *J. Climate,* **17,** 2399–2412.

——, Y.-G. Ham, J.-S. Kug, F.-F. Jin, and I.-S. Kang, 2005: El Niño–La Niña asymmetry in the Coupled Model Intercomparison Project simulations. *J. Climate,* **18,** 2617–2627.

Annamalai, H., K. Hamilton, and K. R. Sperber, 2007: South Asian summer monsoon and its relationship with ENSO in the IPCC AR4 simulations. *J. Climate,* **20,** 1071–1092.

Bjerknes, J., 1969: Atmospheric teleconnections from the equatorial Pacific. *Mon. Wea. Rev.,* **97,** 163–172.

Bretherton, C. S., C. Smith, and J. M. Wallace, 1992: An intercomparison of methods for finding coupled patterns in climate data. *J. Climate,* **5,** 541–560.

Chang, C.-P., Z. Wang, J. McBride, and C.-H. Liu, 2005: Annual cycle of Southeast Asia–Maritime Continent rainfall and the asymmetric monsoon transition. *J. Climate,* **18,** 287–301.

Chen, M., P. Xie, J. E. Janowiak, and P. A. Arkin, 2002: Global land precipitation: A 50-yr monthly analysis based on gauge observations. *J. Hydrometeor.,* **3,** 249–266.

Chikira, M., 2010: A cumulus parameterization with state-dependent entrainment rate. Part II: Impact on climatology in a general circulation model. *J. Atmos. Sci.,* **67,** 2194–2211.

——, and Sugiyama, M., 2010: A cumulus parameterization with state-dependent entrainment rate. Part I: Description and sensitivity to temperature and humidity profiles. *J. Atmos. Sci.,* **67,** 2171–2193.

Collins, M., and Coauthors, 2010: The impact of global warming on the tropical Pacific Ocean and El Niño. *Nat. Geosci.,* **3,** 391–397.

Guilyardi, E., A. Wittenberg, A. Fedorov, M. Collins, C. Wang, A. Capotondi, G. J. van Oldenborgh, and T. Stockdale, 2009: Understanding El Niño in ocean–atmosphere general circulation models: Progress and challenges. *Bull. Amer. Meteor. Soc.,* **90,** 325–340.

Jin, E. K., and Coauthors, 2008: Current status of ENSO prediction skill in coupled ocean–atmosphere model. *Climate Dyn.,* **31,** 647–664.

Jin, F.-F., S.-I. An, A. Timmermann, and J. Zhao, 2003: Strong El Niño events and nonlinear dynamical heating. *Geophys. Res. Lett.,* **30,** 1120, doi:10.1029/2002GL016356.

Joseph, R., and S. Nigam, 2006: ENSO evolution and teleconnections in IPCC's twentieth-century climate simulations: Realistic representation? *J. Climate,* **19,** 4360–4377.

Kanamitsu, M., W. Ebisuzaki, J. Woollen, S.-K. Yang, J. J. Hnilo, M. Fiorino, and G. L. Potter, 2002: NCEP–DOE AMIP-II Reanalysis (R-2). *Bull. Amer. Meteor. Soc.,* **83,** 1631–1643.

Kim, H.-J., B. Wang, and Q. Ding, 2008: The global monsoon variability simulated by CMIP3 coupled climate models. *J. Climate,* **21,** 5271–5294.

Latif, M., and Coauthors, 2001: ENSIP: The El Niño Simulation Intercomparison Project. *Climate Dyn.,* **18,** 255–276.

Lau, K.-M., and S. Yang, 2003: Walker circulation. *Encyclopedia of Atmospheric Sciences,* J. R. Holton, J. A. Pyle, and J. A. Curry, Eds., Academic Press, 2505–2510.

Lin, J.-L., 2007: Interdecadal variability of ENSO in 21 IPCC AR4 coupled GCMs. *Geophys. Res. Lett.,* **34,** L12702, doi:10.1029/2006GL028937.

Mechoso, C. R., and Coauthors, 1995: The seasonal cycle over the tropical Pacific in coupled ocean–atmosphere general circulation models. *Mon. Wea. Rev.,* **123,** 2825–2838.

Neelin, J. D., and Coauthors, 1992: Tropical air-sea interaction in general circulation models. *Climate Dyn.,* **7,** 73–104.

Polito, P. S., O. T. Sato, and I. Wainer, 2008: Height variability from the MIROC–IPCC model for the 20th century compared

to that of the TOPEX/POSEIDON altimeter. *Ocean Modell.,* **24,** 73–91.

Shiogama, H., A. Hasegawa, T. Nozawa, and S. Emori, 2008: Changes in mean and extreme precipitation in near-term predictions up to the year 2030. *SOLA,* **4,** 17–20.

Smith, T. M., R. W. Reynolds, T. C. Peterson, and J. Lawrimore, 2008: Improvements to NOAA's historical merged land–ocean surface temperature analysis (1880–2006). *J. Climate,* **21,** 2283–2296.

Sperber, K. R., and T. N., Palmer, 1996: Interannual tropical rainfall variability in general circulation model simulations associated with the Atmospheric Model Intercomparison Project. *J. Climate,* **9,** 2727–2750.

——, and Coauthors, 1999: Are revised models better models? A skill score assessment of regional interannual variability. *Geophys. Res. Lett.,* **26,** 1267–1270.

Sugiyama, M., H. Shiogamab, and S. Emori, 2010: Precipitation extreme changes exceeding moisture content increases in MIROC and IPCC climate models. *Proc. Natl. Acad. Sci. USA,* **107,** 571–575.

Tanaka, M., 1997: Interannual and interdecadal variations of the western North Pacific monsoon and the East Asian Baiu rainfall and their relationship to ENSO cycles. *J. Meteor. Soc. Japan,* **75,** 1109–1123.

Trenberth, K. E., D. P. Stepaniak, and J. M. Caron, 2000: The global monsoon as seen through the divergent atmospheric circulation. *J. Climate,* **13,** 3969–3993.

van Oldenborgh, G. J., S. Y. Philip, and M. Collins, 2005: El Niño in a changing climate: A multi-model study. *Ocean Sci.,* **1,** 81–95.

Vecchi, G. A., and A. T. Wittenberg, 2010: El Niño and our future climate: Where do we stand? *Wiley Interdiscip. Rev.: Climate Change,* **1,** 260–270.

Wang, B., and Q. Ding, 2006: Changes in global monsoon precipitation over the past 56 years. *Geophys. Res. Lett.,* **33,** L06711, doi:10.1029/2005GL025347.

——, and ——, 2008: Global monsoon: Dominant mode of annual variation in the tropics. *Dyn. Atmos. Oceans,* **44,** 165–183.

——, H.-J. Kim, K. Kikuchi, and A. Kitoh, 2011a: Diagnostic metrics for evaluation of annual and diurnal cycles. *Climate Dyn.,* **37,** 941–955, doi:10.1007/s00382-010-0877-0.

Wang, X., D. Wang, and W. Zhou, 2009: Decadal variability of twentieth-century El Niño and La Niña occurrence from observations and IPCC AR4 coupled models. *Geophys. Res. Lett.,* **36,** L11701, doi:10.1029/2009GL037929.

Watanabe, M., and Coauthors, 2010: Improved climate simulation by MIROC5: Mean states, variability, and climate sensitivity. *J. Climate,* **23,** 6312–6335.

——, M. Chikira, Y. Imada, and M. Kimoto, 2011: Convective control of ENSO simulated in MIROC. *J. Climate,* **24,** 543–562.

White, H. G., 1980: Skewness, kurtosis and extreme values of Northern Hemisphere geopotential heights. *Mon. Wea. Rev.,* **108,** 1446–1455.

Wilks, D. S., 1995: *Statistical Methods in the Atmospheric Sciences: An Introduction*. International Geophysics Series, Vol. 59, Academic Press, 467 pp.

Wu, R., and B. Wang, 2000: Interannual variability of summer monsoon onset over the western North Pacific and the underlying processes. *J. Climate,* **13,** 2483–2501.

Xie, P., and P. A. Arkin, 1997: Global precipitation: A 17-year monthly analysis based on gauge observations, satellite estimates, and numerical model outputs. *Bull. Amer. Meteor. Soc.,* **78,** 2539–2558.

Yokohata, T., and Coauthors, 2007: Different transient climate responses of two versions of an atmosphere-ocean coupled general circulation model. *Geophys. Res. Lett.,* **34,** L02707, doi:10.1029/2006GL027966.

Yoshikawa, C., M. Kawamiya, T. Kato, Y. Yamanaka, and T. Matsuno, 2008: Geographical distribution of the feedback between future climate change and the carbon cycle. *J. Geophys. Res.,* **113,** G03002, doi:10.1029/2007JG000570.